ANOTHER LOOK AT STOCHASTIC CONDENSATION IN CLOUDS: EXACT SOLUTIONS, FOKKER-PLANCK APPROXIMATIONS AND ADIABATIC EVOLUTION

Christopher A. Jeffery *
Space and Remote Sensing Sciences (ISR-2), LANL, Los Alamos, NM

Jon M. Reisner & Miroslaw Andrejczuk
Atmospheric, Climate and Environmental Dynamics (EES-2), LANL, Los Alamos, NM

1. INTRODUCTION

One of the most important theoretical constructs in atmospheric science is the gradient transport model for the flux $\overline{\boldsymbol{u}'\zeta'}$,

$$\overline{\boldsymbol{u}'\zeta'} = -K\boldsymbol{\nabla}\overline{\zeta}$$

which enables the derivation of logarithmic profiles of velocity ($\zeta' = w'$) and temperature ($\zeta' = T'$) in the atmospheric surface layer and provides a subgrid closure (eddy viscosity and diffusivity) for atmospheric models. In modern atmospheric texts and treatments, the gradient model is usually postulated a priori. But underlying this model is a rich stochastic framework that, in the earlier years of atmospheric science, was given due consideration. The interested reader is referred to Sutton (1953) for the historical flavor of this discussion.

In fact, the stochastic Langevin equation (Risken 1989) underlying the gradient model is simply

$$\frac{d\boldsymbol{X}}{dt} = \boldsymbol{u}'$$

where $\boldsymbol{X}$ is Lagrangian position and $\boldsymbol{u}'$ is independently distributed with the following constraint: either (i) $\boldsymbol{u}'$ is assumed Gaussian with a renewal time, τ, that is smaller—but not vanishingly smaller—than the macroscopic evolution time, or (ii) $\boldsymbol{u}'$ is arbitrarily distributed with assumed renewal time $\tau \to 0$, the former being the better assumption for turbulent transport. Seen in this light, the gradient model is, of course, a Fokker-Planck operator (Risken 1989).

It is natural, then, to inquire whether this stochastic formulation may have applicability to other subgrid problems, and in the 1960s a group of Russian scientists (Belyaev 1961; Sedunov 1965; Mazin 1965; Levin and Sedunov 1966a,b) postulated

$$\frac{dr}{dt} \sim \frac{S'}{r}$$

where r is droplet radius and S' is a random supersaturation fluctuation with the correlation $\overline{S'f'}$ analogous to the flux $\overline{\boldsymbol{u}'\zeta'}$ where $f(r)$ is the droplet-size density. Appropriately, this theoretical approach has inherited the name "stochastic condensation". Despite the obvious analogy to the ubiquitous eddy-diffusivity parameterization, the investigation of the correlation $\overline{S'f'}$ and its corresponding gradient model, has largely been ignored outside of the Russian community with few exceptions (e.g. Manton (1979); Khvorostyanov and Curry (1999a,b)).

This extended manuscript summarizes the results of Jeffery et al. (2006). In Jeffery et al. and here we take another look at the Langevin equation for droplet growth and its corresponding Fokker-Planck equation, with the overarching goal of clarifying and elucidating stochastic condensation and its applicability to subgrid atmospheric modeling. To this end we begin with a stochastic model, described in Sec. 2, that assumes S' is independently and normally distributed with given time-dependent variance, $\sigma^2(t)$ and fixed renewal time. We do not construct a model for $\sigma^2(t)$, nor do we relate S' to vertical velocity; rather, we treat $\sigma^2(t)$ as externally provided. A discussion of the validity of these modeling assumptions is postponed until their consequences have been deduced. The exact analytic solution to the present model is derived in Sec. 3, and the corresponding Fokker-Planck equation presented in Sec. 4. In Sec. 5, the impact of S'-fluctuations on the mean supersaturation $\overline{S}$ is derived and the coupled evolution of $\{\overline{S}, f\}$ in a closed, adiabatic volume is assessed. We search for evidence of the stochastic condensation mechanism in cloud droplet spectra from cumulus cloud fields in Sec. 7; Sec. 8 contains a summary.

2. THE MODEL

Following the proceeding discussion, we introduce the following exactly solvable model of stochastic condensation and evaporation. The local supersaturation field experienced by the i-th droplet is decomposed

*Corresponding author address: Christopher A. Jeffery, Los Alamos National Laboratory (ISR-2), PO Box 1663, Mail Stop D-436, Los Alamos, NM 87545, USA. Tel.: (505) 665-9169; fax: (505) 664-0362. Email: cjeffery@lanl.gov

into mean, $\overline{S}(t)$, and fluctuating, $S'(i,t)$, components where S' is a centered, independent random variable that obeys a Gaussian law and is renewed after a time, τ, associated with the system (grid-cell) large-eddy turn-over time. This renewal process imparts a discrete nature on the droplet statistics. Let us decompose continuous time, t, into segments of length τ:

$$t = \{(n-1) + \varphi\}\tau \tag{1}$$

where the restriction $\varphi \in [0,1)$ uniquely defines the integer n for a given t. The label n thereby denotes the time interval $(n-1)\tau \leq t < n\tau$ and the corresponding supersaturation S'_n drawn at time $t = (n-1)\tau$ from a Gaussian of variance σ_n^2. With this notation, the two-time statistics of S' are given by

$$\langle S'_m(i,t_1)S'_n(j,t_2)\rangle = \sigma_n^2 \delta_{mn}\delta_{ij} \tag{2}$$

where $\langle\cdot\rangle$ represents an ensemble average over S'. To complete the model we specify the following Langevin equation:

$$\dot{r} = \frac{\alpha(\overline{S} + S')}{r + a} \tag{3}$$

where a is an accommodation length and α is defined in Appendix A.

3. EXACT ANALYTIC SOLUTION

We proceed to calculate the exact transition probability distribution function for a *single* droplet, $G(r,t|r_0)$. This derivation exploits the seminal property that the sum of two independent Gaussian random variables is, itself, a Gaussian random variable. Integrating Eq. (3) gives

$$(r+a)^2 = (r_0+a)^2 + 2\alpha\int_0^t \mathrm{d}\xi\ \overline{S}(\xi) + 2\alpha\lambda(t)\tau \tag{4}$$

where

$$\lambda \equiv \frac{1}{\tau}\int_0^t \mathrm{d}\xi\ S'(\xi)$$

and $r(t=0) = r_0$. It is important to emphasize that Eq. (4) does not incorporate a boundary condition at $r = 0$ that prevents the prediction of negative radii. Thus this equation is only valid for those S' fluctuations that give $r \geq 0$. In terms of G, this restriction demands $G = 0$ for $r < 0$.

The discrete nature of S' appears in the evaluation of λ for the present model:

$$\lambda(t) = \sum_{i=1}^{n-1} S'_i + \varphi S'_n. \tag{5}$$

We can now evaluate the probability distribution $P(\lambda)$ using Eq. (2) and the Gaussian definition.

The first term on the rhs of Eq. (5), denoted λ_0, is normally distributed with zero mean and variance $\sum_{i=1}^{n-1}\sigma_i^2$. The probability of a given λ is therefore the sum of the probabilities of all combinations $\{\lambda_0, \varphi S'\}$ that add to λ:

$$P(\lambda) = \langle P(\lambda_0)P(S')\rangle_{\lambda_0+\varphi S'=\lambda}$$

Computing this expected value we find

$$\begin{aligned} P(\lambda) &= \int_{-\infty}^{\infty}\mathrm{d}S'\frac{1}{\sqrt{2\pi\sum_{i=1}^{n-1}\sigma_i^2}}\exp\left[-\frac{(\lambda-\varphi S')^2}{2\sum_{i=1}^{n-1}\sigma_i^2}\right] \\ &\quad \frac{1}{\sqrt{2\pi}\sigma_n}\exp\left(-\frac{S'^2}{2\sigma_n^2}\right) \\ &= \frac{\exp\left[-\frac{\lambda^2}{2(\sum_{i=1}^{n-1}\sigma_i^2+\varphi^2\sigma_n^2)}\right]}{\sqrt{2\pi(\sum_{i=1}^{n-1}\sigma_i^2+\varphi^2\sigma_n^2)}} \end{aligned} \tag{6}$$

Thus λ is normally distributed with variance $\sum_{i=1}^{n-1}\sigma_i^2 + \varphi^2\sigma_n^2$.

Using Eq. (4) and the relation, $P(r) = (\partial\lambda/\partial r)P(\lambda)$, gives

$$G(r,t|r_0) = \frac{r+a}{\sqrt{\pi\mathcal{D}_{\mathrm{int}}}}\exp\left(-\frac{\Delta^2}{4\mathcal{D}_{\mathrm{int}}}\right) \tag{7}$$

with time-integrated diffusivity

$$\mathcal{D}_{\mathrm{int}}(t) \equiv 2\tau^2\alpha^2\left(\sum_{i=1}^{n-1}\sigma_i^2 + \varphi^2\sigma_n^2\right) \tag{8}$$

and where

$$\Delta \equiv (r+a)^2 - (r_0+a)^2 - 2\alpha\int_0^t \mathrm{d}\xi\overline{S}(\xi)$$

is the difference between $(r+a)^2$ and the value obtained from evolving $(r_0+a)^2$ in time using the mean supersaturation $\overline{S}$.

Equation (7) is the exact analytic solution to the model of Sec. 2. We reiterate that this solution is strictly valid when $G(r<0) = 0$. However, as long as the solution for $r > 0$ retains its full skewed-Gaussian form, i.e. $\lim_{r\to 0} G \ll a(\pi\mathcal{D}_{\mathrm{int}})^{-1/2}$, neglect of the $r = 0$ boundary condition in the derivation of the analytic solution is justified. In practice, this limits the applicability of the present model to those $\{r_0, \overline{S}(t), \mathcal{D}_{\mathrm{int}}(t)\}$ which keep the support of G away from $r = 0$. The discrete nature of the renewal process is evident in the definition of $\mathcal{D}_{\mathrm{int}}$. While the variance of S' may vary continuously in time, the renewal process samples S' at discrete times $t \in \{0, \tau, 2\tau, \ldots, (n-1)\tau\}$.

3a. *Time-independent* σ^2

The connection between Eq. (7) and a diffusive process with diffusivity $\mathcal{D}$ is revealed when the statistics of S' are time-independent. In this case, Eq. (7) becomes

$$G(r,t|r_0) = \frac{r+a}{\sqrt{\pi\mathcal{D}\gamma}} \exp\left(-\frac{\Delta^2}{4\mathcal{D}\gamma}\right) \tag{9}$$

where $\mathcal{D} \equiv 2\tau\alpha^2\sigma^2$ and the time

$$\gamma(t) = \{(n-1)+\varphi^2\}\tau \tag{10}$$

where $\{\varphi, n\}$ are defined implicitly by Eq. (1). Equation (9) has the familiar form of a Green's function solution describing the diffusion of $(r+a)^2$. As expected, $\mathcal{D}$ exhibits a linear dependence on the renewal time, τ, and the S' variance, σ^2.

Inspection of Eqs. (1) and (10) reveals that γ differs from t; this comparison is shown in Fig. 1. The two times agree periodically at every $\varphi = 0$, while at $\varphi = 1/2$, t exceeds γ by $\tau/4$. While γ is continuous in time it is not smooth, and all the statistics of spectral evolution inherit this lack of smoothness.

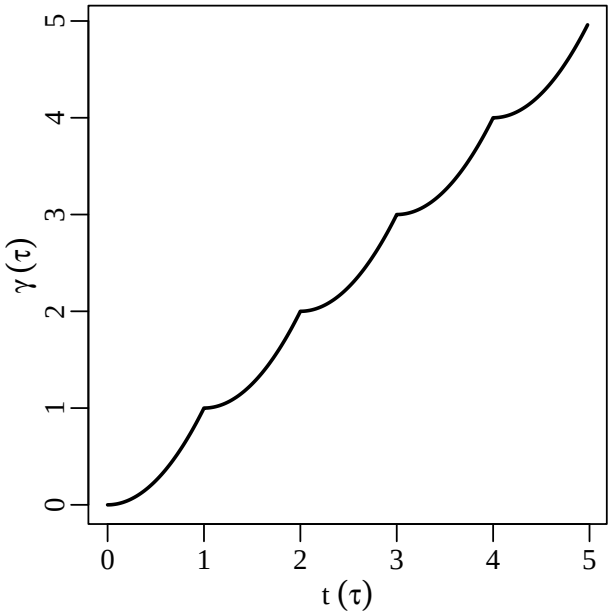

Figure 1: The function $\gamma(t)$, defined by Eq. (10), is continuous but not smooth, and is periodically equal to t when S' is renewed ($\varphi = 0$).

3b. *Droplet population*

For a population of droplets where the S' renewal times are *synchronized*, the droplet-size distribution function, $f(r,t)$, is given by the convolution of G with the initial distribution of sizes, $f_0(r)$:

$$f(r,t) = \int_0^\infty \mathrm{d}r_0 \; f_0(r_0) G(r,t|r_0)$$

The present model is of sufficient generality to incorporate distributions of renewal times that are not synchronized. A pertinent example is the case where the renewal time, τ, is the same for each drop but the first renewal event differs and occurs at a time $\varphi_0\tau$ with $\varphi_0 \in [0,1]$. Evaluation of f now includes a convolution over the initial distribution, $\varphi(\varphi_0)$, of φ_0 values:

$$f(r,t) = \int_{-\infty}^\infty \mathrm{d}r_0 \int_0^1 \mathrm{d}\varphi_0 \; f_0(r_0)\varphi(\varphi_0) G(r,t|r_0,\varphi_0)$$

4. FOKKER-PLANCK APPROXIMATION

The only difference between the behavior of the exact Green's function solution, Eq. (7), for the present model and diffusion of $(r+a)^2$ with a time-dependent diffusivity is the discrete nature of $\mathcal{D}_{\rm int}$ which is exemplified in the behavior of γ shown in Fig. 1. Replacing the discrete, φ^2-weighted sampling of σ^2 by its continuous surrogate gives the Fokker-Planck approximation to the exact solution.

The Fokker-Planck equation describing the evolution of the PDF of $\beta = (r+a)^2$ with drift $2\alpha\overline{S}$ and diffusivity $\mathcal{D}_{\rm FP}$ is

$$\frac{\partial f_{\rm FP}(\beta,t)}{\partial t} = -2\alpha\overline{S}\frac{\partial f_{\rm FP}}{\partial \beta} + \mathcal{D}_{\rm FP}\frac{\partial^2 f_{\rm FP}}{\partial \beta^2}$$

where $\mathcal{D}_{\rm FP}(t) \equiv 2\tau\alpha^2\sigma^2(t)$ is the continuous surrogate to Eq. (8). Straightforward manipulation yields

$$\frac{\partial f_{\rm FP}(r,t)}{\partial t} = -\alpha\overline{S}\frac{\partial}{\partial r}\left(\frac{f_{\rm FP}}{r+a}\right) + \frac{\mathcal{D}_{\rm FP}}{4}\frac{\partial}{\partial r}\frac{1}{(r+a)}\frac{\partial}{\partial r}\frac{f_{\rm FP}}{(r+a)} \tag{11}$$

with Green's function solution

$$G_{\rm FP}(r,t|r_0) = \frac{r+a}{\sqrt{\pi\int_0^t \mathrm{d}\xi \mathcal{D}_{\rm FP}(\xi)}} \exp\left(-\frac{\Delta^2}{4\int_0^t \mathrm{d}\xi \mathcal{D}_{\rm FP}(\xi)}\right) \tag{12}$$

Equations (11) and (12), unlike the exact solution, are smooth. We observe that $G_{\rm FP}$ is equal to G at the renewal times $t = i\tau$. Formally we can derive $G_{\rm FP}$ from G by taking the limit $\tau \to 0$ while holding $\mathcal{D}_{\rm int}$ constant. This renormalization is an approximation that holds when $\tau \ll t$ for all t of interest. The small τ limit does not generally hold for turbulent systems where τ corresponds to the system (grid cell) large-eddy turnover time.

Equations (11) and (12) were first derived by Belyaev (1961), Sedunov (1965), Mazin (1965) and Levin and Sedunov (1966a,b) for $a = 0$. These authors *do not* derive an exact solution and then infer the Fokker-Planck equivalent as we have done here. Rather they use standard methods from Fokker-Planck theory that are available in many texts, e.g. Risken (1989), and are not pursued here. Of further interest, Manton (1979) uses a first order smoothing approximation to derive Eq. (11) from correlated S' fluctuations and the $\tau \to 0$ renormalization.

4a. $\langle S'|r\rangle_{\rm FP}$

The PDF equation for the present model is conveniently written in terms of the conditional quantity $\langle S'|r\rangle$ (Jeffery and Reisner 2006):

$$\frac{\partial f(r,t)}{\partial t} = -\alpha\overline{S}\frac{\partial}{\partial r}\left(\frac{f}{r+a}\right) - \alpha\frac{\partial}{\partial r}\left(\frac{\langle S'|r\rangle\, f}{r+a}\right) \quad (13)$$

Comparison of Eqs. (13) and (11) gives the expression for $\langle S'|r\rangle$ in the Fokker-Planck approximation:

$$\langle S'|r\rangle_{\rm FP} = -\frac{\mathcal{D}_{\rm FP}}{4\alpha}\frac{1}{f_{\rm FP}}\frac{\partial}{\partial r}\left\{\frac{f_{\rm FP}}{(r+a)}\right\} \quad (14)$$

For the special case $f_{\rm FP}$ = $G_{\rm FP}$ and constant σ^2, Eq. (14) gives

$$\langle S'|r\rangle_{{\rm FP},G} = \frac{\Delta}{4\alpha t} \quad (15)$$

4b. *Moments*

Using the definition $\langle\cdot\rangle_r \equiv \int_0^\infty {\rm d}r\ \cdot$, Eq. (11) and assuming all moments exist, integration by parts gives the following equations for the evolution of the r-moments:

$$\begin{aligned}
\frac{d\,\langle r\rangle_r}{dt} &= \alpha\overline{S}\left\langle\frac{1}{r+a}\right\rangle_r - \frac{\mathcal{D}_{\rm FP}}{4}\left\{\frac{f_{\rm FP}(0,t)}{a^2} + \left\langle(r+a)^{-3}\right\rangle_r\right\} \\
\frac{d\langle r^2\rangle_r}{dt} &= 2\alpha\overline{S}\left\langle\frac{r}{r+a}\right\rangle_r + \frac{\mathcal{D}_{\rm FP}}{2}\left\langle\frac{a}{(r+a)^3}\right\rangle_r \\
\frac{d\langle r^3\rangle_r}{dt} &= 3\alpha\overline{S}\left\langle\frac{r^2}{r+a}\right\rangle_r + \frac{3\mathcal{D}_{\rm FP}}{4}\left\langle\frac{r(r+2a)}{(r+a)^3}\right\rangle_r
\end{aligned} \quad (16)$$

valid for $a > 0$. These equations reveal that the impact of S'-fluctuations on the evolution of the first three moments depends strongly on f in the "small r" region $r \le a$. In particular, for narrow spectral support, $\overline{S} > 0$ and fixed $\{\overline{S}, \mathcal{D}_{\rm FP}\}$, the $\overline{S}$-term increasingly dominates the diffusion term as the spectrum grows to larger sizes.

5. ADIABATIC EVOLUTION OF $\overline{S}$

The early studies of stochastic condensation and evaporation neglected the impact of S' on the adiabatic evolution of $\overline{S}$, e.g. (Levin and Sedunov 1967). The first self-consistent derivation of evolution equations for both $\overline{S}$ and f in terms of a single diffusivity, $\mathcal{D}_{\rm FP}$, was performed by Voloshchuk and Sedunov (1977). Voloshchuk and Sedunov used approximate methods to derive the S' contribution to the f-equation. But an error in their derivation that was subsequently "canceled" by a first-order Taylor series approximation lead Voloshchuk and Sedunov to the exact result.

5a. $\sigma^2 = 0$

We first consider the evolution of $\overline{S}$ of a closed, well-mixed, adiabatic parcel with a non-disperse population of droplets of size r_0 at $t = 0$; this analysis lays the foundation for the $\sigma^2 \ne 0$ case considered subsequently. For this study, we ignore the dependence of droplet activation on supersaturation and assume that the parcel contains a given number of droplets at $t = 0$. This is a classical problem in cloud physics that has been studied since the 1950s.

The equation for $\overline{S}$ for the present scenario is

$$\frac{d\overline{S}}{dt} = c_1\overline{w}(t) - c_2\frac{dr^3}{dt} \quad (17)$$

where c_1 and c_2 are defined in Appendix A. Using the well-known quasi-stationary (QS) assumption, $d\overline{S}/dt = 0$ corresponding to the low-frequency behavior of $\overline{S}$, and integrating Eq. (17) gives

$$r^3 = r_0^3 + a^3 N_z(t)$$

where

$$N_z(t) \equiv \frac{c_1}{c_2 a^3} z(t)$$

and $z(t) = \int_0^t {\rm d}\xi\ \overline{w}(\xi)$. The non-dimensional number N_z determines the linear relationship between liquid water and height $z(t)$.

Substitution of $\mathcal{B}_{\rm QS} = (r+a)^2/a^2$ gives

$$\left(\mathcal{B}_{\rm QS}^{1/2} - 1\right)^3 = \frac{r_0^3}{a^3} + N_z(t) \quad (18)$$

The non-dimensional variable $\mathcal{B}_{\rm QS}$ is relevant because $\overline{S}_{\rm QS} = a^2/(2\alpha)d\mathcal{B}_{\rm QS}/dt$ from Eq. (4). Introducing a second non-dimensional number

$$N_w(t) \equiv \frac{c_1}{c_2 a\alpha}\overline{w}(t)$$

and solving for $\overline{S}_{\rm QS}$ gives

$$\overline{S}_{\rm QS} = \frac{N_w}{3}\left(\frac{r_0^3}{a^3} + N_z\right)^{-2/3}\left\{1 + \left(\frac{r_0^3}{a^3} + N_z\right)^{1/3}\right\}$$

which illustrates how the two numbers $\{N_z, N_w\}$ combine to modulate $\overline{S}$. For the special case of constant $\overline{w}$ we have the asymptotic

$$\lim_{N_z\to\infty} \overline{S}_{\rm QS} \sim N_z^{-1/3} \sim t^{-1/3}$$

which shows that $\overline{S}_{\rm QS}$ decays as the parcel rises. For the regime $r_0^3/a^3 \ll N_z \ll 1$ we have

$$\overline{S}_{\rm QS} \sim N_z^{-2/3} \sim t^{-2/3}$$

which exhibits a faster decay.

5b. $\sigma^2 \neq 0$

We now consider the evolution of $\langle \overline{S} \rangle$ of a closed, well-mixed, adiabatic parcel with S' fluctuations using the model of Sec. 2. In this case the evolution equation for $\langle \overline{S} \rangle$ includes a contribution from S' which we write in two equivalent ways:

$$\begin{aligned}
\frac{d\langle \overline{S}\rangle}{dt} &= c_1\overline{w}(t) - c_2\left\langle \frac{d\langle r^3\rangle_r}{dt}\right\rangle \\
&= c_1\overline{w}(t) - 3\alpha c_2\left\{\left\langle\frac{r^2}{r+a}\right\rangle_r \langle\overline{S}\rangle + \left\langle\left\langle\frac{r^2}{r+a}\middle| S'\right\rangle_r\right\rangle\right\} \qquad (19a)\\
&= c_1\overline{w}(t) - 3\alpha c_2\left\{\left\langle\frac{r^2}{r+a}\right\rangle_r \langle\overline{S}\rangle + \left\langle\frac{r^2}{r+a}\langle S'|r\rangle\right\rangle_r\right\} \qquad (19b)
\end{aligned}$$

It is important to emphasize that there are two distinct averaging procedures that appear in Eq. (19): the $\langle\cdot\rangle$ average over an ensemble of S' fluctuations and the $\langle\cdot\rangle_r$ average over $f(r)$. The only difference between Eqs. (19a) and (19b) is the order in which the averaging is performed. We have already discussed the conditional average $\langle S'|r\rangle$ in some detail and will proceed to evaluate Eq. (19b) using the Fokker-Planck approximation.

Substitution of the Fokker-Planck expression, $\langle S'|r\rangle_{\rm FP}$, into Eq.(19b) and integration by parts gives

$$\frac{d\overline{S}_{\rm FP}}{dt} = c_1\overline{w}(t) - 3\alpha c_2\left\{\left\langle\frac{r^2}{r+a}\right\rangle_r \overline{S}_{\rm FP} + \frac{\mathcal{D}_{\rm FP}}{4\alpha}\left\langle\frac{r(r+2a)}{(r+a)^3}\right\rangle_r\right\} \qquad (20)$$

valid for $a > 0$. Eqs. (11) and (20) form two coupled, self-consistent equations that describe the evolution of $\{f_{\rm FP}, \overline{S}_{\rm FP}\}$ in a closed, adiabatic parcel. As a consistency check we note that the new (3rd) term on the rhs of Eq. (20) could have also been derived by simply substituting Eq. (16) for $d\langle r^3\rangle_r/dt$ directly into $d\overline{S}_{\rm FP}/dt = c_1\overline{w} - c_2 d\langle r^3\rangle_r/dt$. Clearly, Eqs. (11) and (20) conserve total water. For $a = 0$ a similar result was first derived by Voloshchuk and Sedunov (1977) using an incorrect method.

5c. $\overline{S}_{\rm FP,QS}$

The QS evaluation of $\overline{S}_{\rm FP}$ from Eq. (20) is

$$\overline{S}_{\rm FP,QS} = \frac{c_1\overline{w}(t)}{3\alpha c_2}\left\langle\frac{r^2}{r+a}\right\rangle_r^{-1}\left\{1 - \frac{\mathcal{D}_{\rm FP}}{4}\frac{3c_2}{c_1\overline{w}(t)}\langle J\rangle_r\right\} \qquad (21)$$

valid for $a > 0$ where $J = r(r+2a)/(r+a)^3$. This result shows that the presence of S'-fluctuations in a closed cell—as prescribed by the present model—acts to decrease $\overline{S}_{\rm FP}$. In the language of Cooper (1989, pp. 1306), this occurs because high-$\langle r\rangle_r$ regions tend to have $S' > 0$ and low-$\langle r\rangle_r$ regions have $S' < 0$. However, in contrast to Cooper who associates smaller $\overline{S}_{\rm QS}$ values with a trend toward evaporation and larger $\overline{S}_{\rm QS}$ values with a trend toward enhanced growth, we maintain that the net effect of S'-fluctuations on droplet evolution arises from the coupled impact of $\mathcal{D}_{\rm FP}$ on $\{f_{\rm FP}, \overline{S}_{\rm FP}\}$ and not $\overline{S}_{\rm FP}$ alone. In particular, decreasing $\overline{S}_{\rm FP}$ with increasing $\mathcal{D}_{\rm FP}$ does not necessarily imply a trend toward cloud evaporation.

The impact of S'-fluctuations on $\overline{S}_{\rm FP,QS}$ depends on $f_{\rm FP}$ via the spectral moment $\langle J\rangle_r$. A plot of $\langle J\rangle_r$ vs $\langle r\rangle_r$ is shown in Fig. 2 for three different $f_{\rm FP}$. The figure demonstrates that $\langle J\rangle_r$ peaks in the vicinity of $\langle r\rangle_r = a$ where a is typically around 2 μm.

5d. *Exact solution for* $\overline{S}_{\rm FP,G}$

Using the QS approximation, the coupled behavior of $\{\overline{S}_{\rm FP}, f_{\rm FP}\}$ can be solved exactly for $f_{\rm FP} = G_{\rm FP}$ ignoring boundary effects. $\overline{S}_{\rm FP,G}$ is defined implicitly by the relation

$$\langle r^3\rangle_r = r_0^3 + a^3 N_z(t) \qquad (22)$$

To reveal the other non-dimensional numbers that determine the impact of S'-fluctuations on $\overline{S}_{\rm FP}$, it is helpful to consider the limit $\int_0^t d\xi\ \mathcal{D}_{\rm FP}(\xi)/\beta^2 \ll 1$ where $\beta = (r_0+a)^2 + 2\alpha\int_0^t d\xi\,\overline{S}_{\rm FP,G}(\xi)$ and $\beta > 0$. In this case, a first-order Taylor series expansion in small parameter $\int_0^t d\xi\,\mathcal{D}_{\rm FP}(\xi)/\beta^2$ gives

$$\begin{aligned}
\langle r^3\rangle_r &= \beta^{3/2}\left\{1 + \frac{3\int_0^t d\xi\,\mathcal{D}_{\rm FP}(\xi)}{4\beta^2}\right\} - 3a\beta \\
&\quad + 3a^2\beta^{1/2}\left\{1 - \frac{\int_0^t d\xi\,\mathcal{D}_{\rm FP}(\xi)}{4\beta^2}\right\} - a^3
\end{aligned}$$

Substituting above and rearranging gives

$$\left(\mathcal{B}_{\rm QS}^{1/2} - 1\right)^3 = \frac{r_0^3}{a^3} + N_z\left\{1 - \frac{3}{4}\frac{N_{\mathcal{D}}}{\mathcal{B}_{\rm QS}^{1/2}} + \frac{3}{4}\frac{N_{\mathcal{D}}}{\mathcal{B}_{\rm QS}^{3/2}}\right\} \qquad (23)$$

where

$$N_{\mathcal{D}}(t) \equiv \frac{c_2}{c_1}\frac{\int_0^t d\xi\,\mathcal{D}_{\rm FP}(\xi)}{az(t)} \qquad (24)$$

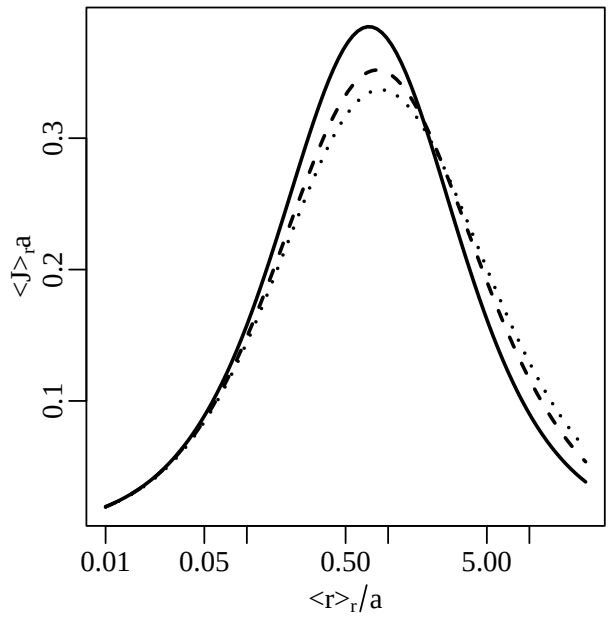

Figure 2: Comparison of $\langle J \rangle_r$ as a function of $\langle r \rangle_r$ computed from three distributions: the gamma function $f_{\rm FP} \sim r^n e^{-(n+1)r/\langle r \rangle_r}$ with $n = 1$ ($\cdots$) and $n = 2$ (- -), and a non-disperse spectrum $f_{\rm FP} = \delta(r - \langle r \rangle_r)$ corresponding to the limit $n \to \infty$ (—). $\langle J \rangle_r$ peaks in the vicinity of $\langle r \rangle_r = a$ for all three $f_{\rm FP}$.

and $\mathcal{B}_{\rm QS} = \beta/a^2$. The number $N_{\mathcal{D}}$ is thus the ratio of two time-integrated forcing terms in the $\overline{S}_{\rm FP}$ evolution equation—diffusion ($c_2 \mathcal{D}_{\rm FP}/a$) and velocity ($c_1 \overline{w}$)—and, as Eq. (23) reveals, $N_{\mathcal{D}}$ determines the relative impact of S'-fluctuations on $\mathcal{B}_{\rm QS}$. Note that when both $\{\overline{w}, \mathcal{D}_{\rm FP}\}$ are constant, $N_{\mathcal{D}} = c_2 \mathcal{D}_{\rm FP}/(c_1 a \overline{w})$ is also constant. If either $\overline{w}$ or $\mathcal{D}_{\rm FP}$ is time-dependent then the number

$$N_{\mathcal{D},\overline{S}} \equiv \frac{c_2 a}{c_1 \alpha} \frac{\mathcal{D}_{\rm FP}(t)}{z(t)},$$

along with N_w, determines the relationship between $\overline{S}$ and $\{\mathcal{B}_{\rm QS}, N_z, N_{\mathcal{D}}\}$.

A contour plot of $\mathcal{B}_{\rm QS}$ as a function of $\{N_z, N_{\mathcal{D}}\}$ calculated from Eq. (22) is shown in Fig. 3(a) for $r_0 = 0$ and $f_{\rm FP} = G_{\rm FP}$. Since $N_z \sim z(t)$ it is useful to note that the time-scale $c_2 a^3/(c_1 \overline{w})$ is of order 1 second for typical atmospheric temperatures, droplet concentrations and updraft velocities. Thus the abscissa of Fig. 3 maps closely to time in seconds for constant $\overline{w}$.

For $N_{\mathcal{D}} = 0$, $\mathcal{B}_{\rm QS}$ increases monotonically with increasing N_z as shown in the bottom of Fig. 3(a) and as indicated by Eq. (18). The figure also shows that $\mathcal{B}_{\rm QS}$ decreases with increasing $N_{\mathcal{D}}$ at fixed N_z; this result is consistent with Eq. (23). In addition, the figure indicates a shaded region where $d\mathcal{B}_{\rm QS}/dN_z < 0$ and, consequently, $\overline{S}_{\rm FP,G} < 0$. The "triple-point" that marks the beginning of this negative $\overline{S}_{\rm FP,G}$ region is $\{N_{\mathcal{D}} \approx 6.5, N_z \approx 0.15, \mathcal{B}_{\rm QS} \approx 1.5\}$. Thus the possibility of negative $\overline{S}_{\rm FP,G}$ in a closed, adiabatic updraft with internal S' fluctuations which was suggested by Eq. (21) is verified for $f_{\rm FP} = G_{\rm FP}$ in Fig. 3(a). Also shown in the figure are three dashed lines that represent predicted distributions where the fraction of droplets with $r \geq 0$ is in the set $\{0.7, 0.8, 0.9\}$. These lines divide the figure into two qualitative regimes: the upper-right region where the boundary condition imposed at $r = 0$ may impact $\mathcal{B}_{\rm QS}$ and the remaining region where this boundary-condition has little impact. The lines suggest that the prediction of negative $\overline{S}_{\rm FP,G}$ is insensitive to this bc for $N_z < 0.15$.

Corresponding values of $\langle r \rangle_r /a$ are reproduced in Fig. 3(b) where the shaded $\overline{S}_{\rm FP,G} < 0$ region and dashed lines are again shown. In contrast to $\mathcal{B}_{\rm QS}$, $\langle r \rangle_r /a$ exhibits a monotonic dependence on $\{N_z, N_{\mathcal{D}}\}$: $\langle r \rangle_r /a$ increases with increasing N_z and decreases with increasing $N_{\mathcal{D}}$. In the region where $\overline{S}_{\rm FP,G} < 0$, $\langle r \rangle_r$ falls between $0.1a$ and $1.25a$; these values are consistent with the behavior of $\langle J \rangle_r$ shown in Fig. 2 and the discussion of Sec. 5c. Moreover, no noticeable changes in the trend of $\langle r \rangle_r$ are seen in the $\overline{S}_{\rm FP,G} < 0$ region. This re-emphasizes that the transition from $\overline{S}_{\rm FP,G} > 0$ to $\overline{S}_{\rm FP,G} < 0$ should not be associated with a qualitative transition from growth to evaporative behavior.

5e. *Summary*

Following the pioneering work of Voloshchuk and Sedunov (1977), we consider the impact of S'-fluctuations, as prescribed by the model of Sec. 2, on the evolution of a closed, adiabatic parcel. This problem lends itself to non-dimensional analysis and to the identification of a finite set of time-dependent non-dimensional numbers that specify the coupled evolution of $\{f_{\rm FP}, \overline{S}_{\rm FP}\}$. Since it is the time integral of $\overline{S}_{\rm FP}$, and not $\overline{S}_{\rm FP}$ itself, that controls the evolution of $f_{\rm FP}$, we identify the set of numbers that determine the evolution of $\{f_{\rm FP}, \mathcal{B}_{\rm QS} \sim \int_0^t \mathrm{d}\xi \; \overline{S}_{\rm FP}(\xi)\}$ and those that diagnose $\overline{S}_{\rm FP}$, separately. This is shown in Table 1 for $f_{\rm FP} = G_{\rm FP}$ and the QS limit. Of particular importance is the number $N_{\mathcal{D}}$, Eq. (24), which controls the impact of S'-fluctuations on the evolution of $\{G_{\rm FP}, \mathcal{B}_{\rm QS}\}$. This number increases with increasing $\mathcal{D}_{\rm FP}$ as expected, but it also decreases with increasing $\overline{w}$, in agreement with concerns raised by Manton (1979, pp. 902) that large updraft velocities decrease the relative importance of

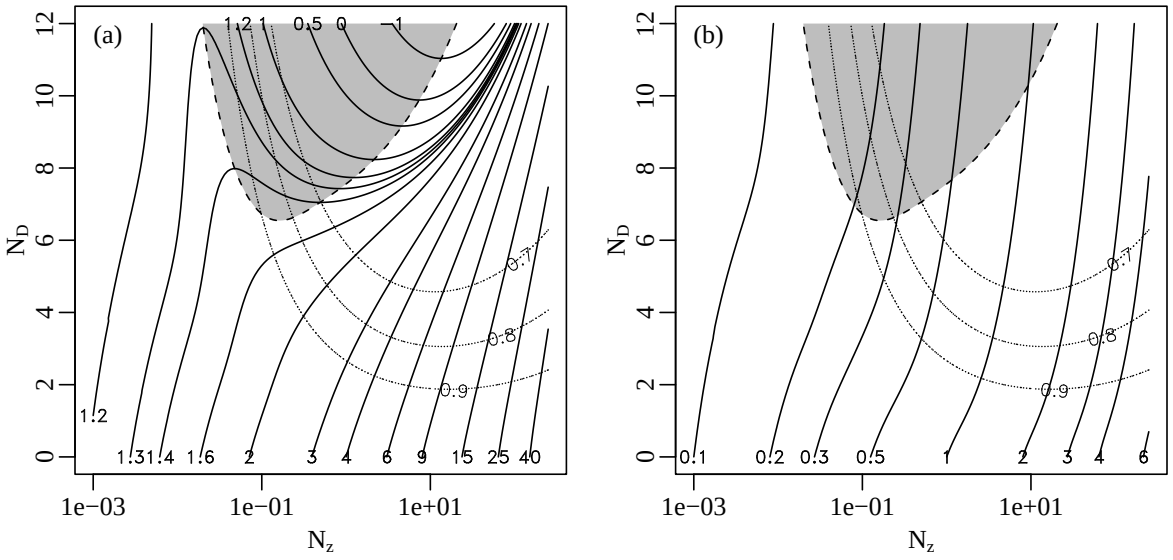

Figure 3: Contour plots of $\mathcal{B}_{\rm QS}$ [3(a)] and $\langle r \rangle_r / a$ [3(b)] as a function of $\{N_z, N_{\mathcal{D}}\}$ calculated from Eqs. (22) with $r_0 = 0$, and indicated by the solid lines. The region where $d\mathcal{B}_{\rm QS}/dN_z < 0$ and, consequently, $\overline{S}_{\rm FP,G} < 0$ is shaded and bounded with a dashed line. Also shown is the cloudy fraction $\langle r^0 \rangle_r \in \{0.7, 0.8, 0.9\}$ indicated by the dotted contours. No noticeable trend toward evaporation is found in the behavior of $\langle r \rangle_r$ in the $\overline{S}_{\rm FP,G} < 0$ region.

S'-fluctuations. Formally, $N_{\mathcal{D}} \sim z^{-1}(t)$; a similar algebraic dependence is found in the results of Cooper (1989, Eq. (10)) in his evaluation of a turbulent correction to $\mathcal{B}_{\rm QS}$. However, the additional dependence $N_{\mathcal{D}} \sim a^{-1}$ is, perhaps, surprising and indicates the importance of regularizing the growth law $dr/dt \sim r^{-1}$ in the limit $r \to 0$.

	$G_{\rm FP}(r, t, \mathcal{B}_{\rm QS} \vert r_0)$	$\overline{S}_{\rm FP,QS}$
$\mathcal{D}_{\rm FP} = 0$	N_z	N_w
$\mathcal{D}_{\rm FP} \neq 0$	N_z, $N_{\mathcal{D}}$	N_w, $N_{\mathcal{D},\overline{S}}$

Table 1: Enumeration of the time-dependent nondimensional numbers that determine $\{G_{\rm FP}, \mathcal{B}_{\rm QS}\}$ in the QS limit, and those that, subsequently, diagnose $\overline{S}_{\rm FP,QS}$. Note that $N_{\mathcal{D},\overline{S}}$ is not relevant when both $\{\mathcal{D}_{\rm FP}, \overline{w}\}$ are constant.

The range of $N_{\mathcal{D}}$ for typical atmospheric conditions and model grid scales is difficult to ascertain because the magnitude and parametric dependencies of the S'-variance, σ^2, are not well understood, and $N_{\mathcal{D}}$, itself, is time-dependent. Passive scalar theory suggests $\sigma^2 \sim L^{2/3}$ in the inertial-convective subrange where L is the grid-cell length, but this estimate is questionable since condensation damps large positive S' fluctuations. Here we choose to estimate $N_{\mathcal{D}}$ assuming time-independent $\{\overline{w}, \mathcal{D}_{\rm FP}\}$ and $\sigma = 0.01$, independent of L, while we retain Kolmogorov scaling for the renewal time, $\tau = 0.1\varepsilon^{-1/3}L^{2/3}$, where ε is the kinetic energy dissipation rate. Two contour plots of $N_{\mathcal{D}}$ are shown in Fig. 4 for $\overline{w} = 1\ {\rm m/s}$ and $\varepsilon = 0.01\ {\rm m^2\ s^{-3}}$, with 4(a) assuming an in-cloud droplet concentration of $N_c = 50\ {\rm cm^{-3}}$ while 4(b) assumes $500\ {\rm cm^{-3}}$. The figures reveal that $N_{\mathcal{D}}$ spans four orders of magnitude in the range 10^{-2} to 10^2 for a broad range of conditions, and increases with temperature and grid-cell length when σ^2 is assumed constant. In particular, an indirect aerosol effect is observed with $N_{\mathcal{D}}$ increasing linearly with N_c at fixed σ^2.

6. SPECTRAL BROADENING

Although Voloshchuk and Sedunov (1977) provide the first self-consistent derivation of coupled equations for $\{f_{\rm FP}, \overline{S}_{\rm FP}\}$ in terms of a single diffusivity, $\mathcal{D}_{\rm FP}$, they do not analyze the resulting spectra. Subsequent studies, e.g. Manton (1979), Khvorostyanov (1988), Khvorostyanov and Curry (1999a,b), that contain a more detailed spectral analysis neglect the impact of

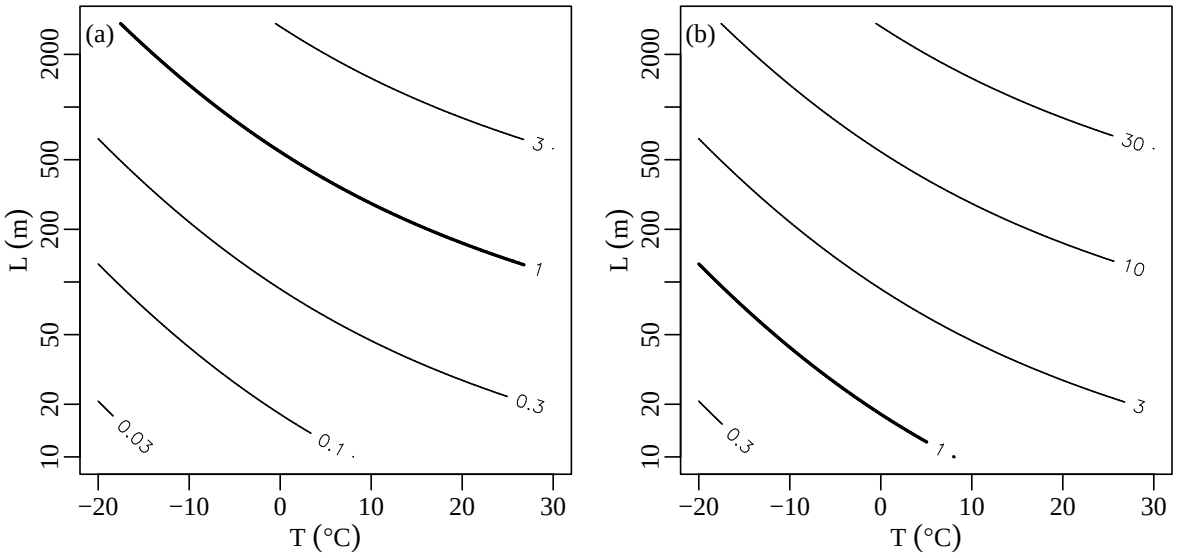

Figure 4: Contour plots of $N_{\mathcal{D}}$ as a function of $\{T, L\}$ for $N_c = 50\ \mathrm{cm}^{-3}$ [Fig. 4(a)] and $N_c = 500\ \mathrm{cm}^{-3}$ [4(b)], typical of clean marine and polluted marine/continental environments, respectively (Heymsfield and McFarquhar 2001). $N_{\mathcal{D}}$ is computed from Eq. (24), assuming $\sigma = 0.01$, $\overline{w} = 1\ \mathrm{m/s}$, the Kolmogorov estimate $\tau = 0.1\varepsilon^{-1/3}L^{2/3}$ and $\varepsilon = 0.01\ \mathrm{m}^2\ \mathrm{s}^{-3}$. The figures reveal that a range of $N_{\mathcal{D}}$ values between 10^{-2} and 10^2 exist for typical atmospheric conditions and model grid sizes.

S'-fluctuations on $\overline{S}_{\mathrm{FP}}$, and therefore, do not conserve liquid water mass. These studies systematically overestimate $\overline{S}_{\mathrm{FP}}$ and, thereby overestimate $\langle r^3 \rangle_r$ and all higher order moments.

Consistent with earlier work (Manton 1979), our closed, adiabatic treatment of $\{f_{\mathrm{FP}}, \overline{S}_{\mathrm{FP}}\}$ in the absence of droplet coalescence produces a relatively small broadening to larger sizes. This is illustrated in Table 2 which lists the relative impact of $N_{\mathcal{D}}$ on $\langle r^6 \rangle_r$; the moment $\langle r^6 \rangle_r$ is of microphysical relevance because it is roughly proportional to precipitation efficiency. For the present comparison, $N_{\mathcal{D}} = 0$ is a single-valued spectrum (zero dispersion) and therefore the calculated increase in $\langle r^6 \rangle_r$ is an upper bound.

In the analysis of Manton (1979, pp. 902), the spectral width of the transition probability G_{FP}, Eq. (12), is shown to follow

$$\lim_{t\to\infty} \Delta r \sim \left\{ \frac{\int_0^t \mathrm{d}\xi\ \mathcal{D}_{\mathrm{FP}}(\xi)}{\alpha \int_0^t \mathrm{d}\xi\ \overline{S}(\xi)} \right\}^{1/2}$$

for $\overline{S} > 0$. Manton further assumes constant $\{\mathcal{D}_{\mathrm{FP}}, \overline{S}\}$ which gives constant Δr and dispersion $\Delta r / \langle r \rangle_r \sim t^{-1/2}$. These estimates are inconsistent with the results of Table 2 which indicate broadening that persists to $r_{\mathrm{vol}} = 50\ \mu\mathrm{m}$. The difference between Manton (1979)'s assumed constant $\overline{S}$ and the asymptotic $\overline{S}_{\mathrm{FP}} \sim t^{-1/3}$ of our closed, adiabatic parcel is the origin of this discrepancy. For the simulations that produced the results of Table 2, Δr broadens slowly with time as $t^{1/6}$ while the dispersion decreases slowly as $t^{-1/6}$.

$N_{\mathcal{D}}$ \ r_{vol}	$\langle r^2 \rangle_r$			$\langle r^6 \rangle_r$		
	10	20	50	10	20	50
1	0.93	0.96	0.98	1.6	1.3	1.2
3	0.84	0.89	0.94	2.4	1.9	1.5
10	0.71	0.77	0.85	4.5	3.2	2.2
30	0.61	0.65	0.74	8.7	5.8	3.7

Table 2: Table of $\langle r^2 \rangle_r (N_{\mathcal{D}}) / \langle r^2 \rangle_r (0)$ (middle column) and $\langle r^6 \rangle_r (N_{\mathcal{D}}) / \langle r^6 \rangle_r (0)$ (right column) calculated at $r_{\mathrm{vol}} \in \{10, 20, 50\}\ \mu\mathrm{m}$ and $N_{\mathcal{D}} \in \{1, 3, 10, 30\}$ with $r_0 = 0$, $\tau_{\mathrm{r}} = 0.025\ \mathrm{s}$ and $N_w = 0.035$. Impact of S'-fluctuations persist to $r_{\mathrm{vol}} = 50\ \mu\mathrm{m}$; the asymptotic decay $\overline{S}_{\mathrm{FP,G}} \sim t^{-1/3}$ of a closed, adiabatic parcel enhances spectral dispersion as compared to earlier estimates (Manton 1979).

We have observed a new effect of the stochastic approach of Levin-Sedunov-Mazin which only appears when the $\overline{S}_{\mathrm{FP}}$ equation is correctly averaged and liq-

uid water mass is exactly conserved. Namely, in a closed, adiabatic parcel, $\langle r^2 \rangle_r$ decreases with increasing $N_{\mathcal{D}}$ at fixed $r_{\rm vol}$ as indicated in Table 2. The significance of this observation is that $\langle r^2 \rangle_r$ is proportional to the shortwave scattering coefficient. Thus stochastic condensation provides a mechanism for decreasing grid-averaged cloud short-wave reflectivity while keeping cloud amount unchanged. However, we reiterate that the results of Table 2 are an upper bound and, furthermore, droplet coalescence may act to mitigate this effect.

Table 2 shows that normalized $\langle r^2 \rangle_r$ decreases with decreasing $r_{\rm vol}$, but this trend does not continue as $r_{\rm vol} \to 0$. The minimum value of normalized $\langle r^2 \rangle_r (N_{\mathcal{D}})$ is shown in Fig. 5 for four values of N_w corresponding to four different droplet concentrations. A few representative values of $r_{\rm vol}(N_{\mathcal{D}})$ are also shown along each of the four lines. Figure 5 reiterates that the impact of S'-fluctuations on droplet spectral evolution becomes significant for $N_{\mathcal{D}}$ values greater than unity and increases monotonically with increasing $N_{\mathcal{D}}$. Minimum values of normalized $\langle r^2 \rangle_r$ occur for $r_{\rm vol}$ in the range 4–14 μm which is of particular significance for cloud shortwave radiative properties. In fact, a survey of effective droplet radius for liquid water clouds using ISCCP satellite observations finds a globally and annually average value of 11.4 ± 5.6 μm (Han et al. 1994), which is precisely the size regime where S'-fluctuations have a maximal impact on $\langle r^2 \rangle_r$.

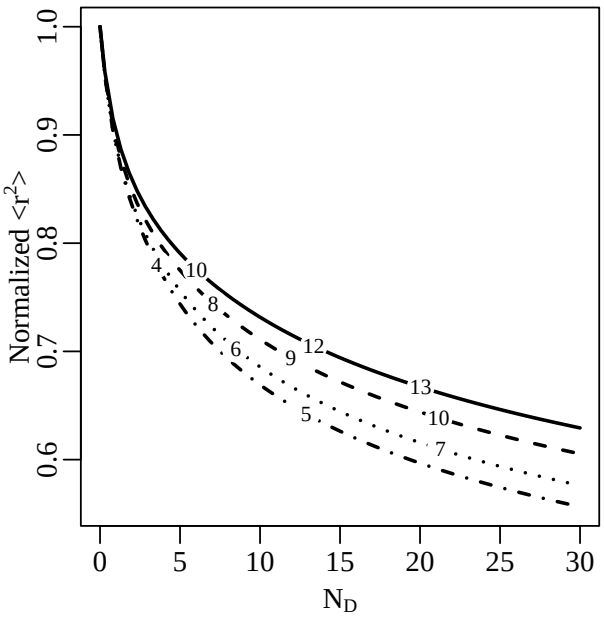

Figure 5: Comparison of the minimum value of $\langle r^2 \rangle_r (N_{\mathcal{D}}) / \langle r^2 \rangle_r (0)$ computed with $r_0 = 0$, $\tau_{\rm r} = 0.025$ s and for four different N_w values: 0.07 (—), 0.035 (- -), 0.014 ($\cdots$) and 0.007 ($\cdot$ – $\cdot$), corresponding to $N_c \in \{50, 100, 250, 500\}\,{\rm cm}^{-3}$, respectively, with $T = 285$ K, and $\overline{w} = 1\,{\rm m/s}$. Also shown are representative values of $r_{\rm vol}$ in μm superimposed on each line.

7. COMPARISON WITH RICO AND SCMS

Underpinning the stochastic approach of Levin-Sedunov-Mazin is the assumption that the cloud droplet spectrum experiences a complete ensemble of S'-fluctuations. This assumption does not hold for a single cloud parcel with given cloud-base properties that rises stochastically to a given height (Bartlett and Jonas 1972). Recent numerical simulations show that fluctuations in microphysical properties occur below the scale of the parcel, but are small and cause little spectral broadening (Vaillancourt et al. 2001, 2002). Observational studies of droplet spectra and correlations, performed on a cloud-by-cloud basis, reveal evidence of stochastic broadening but are far from definitive. For example, the correlation $\langle \langle r \rangle'_r \, w' \rangle$ from a single horizontal transect through a cumulus cloud shows considerable scatter (Austin et al. 1985), but the mean value is uncertain and this statistic, itself, is disputable because it does not include S'-fluctuations associated with temperature/moisture variability and horizontal mixing (Politovich 1993).

A seminal feature of the present analysis is the prediction that $\mathcal{D}_{\rm FP}$, and hence $N_{\mathcal{D}}$, increases with scale, L, as demonstrated in Fig. 4. This hypothesis underpins our analysis of cloud droplet spectra from two observational campaigns: Rain In Cumulus over the Ocean (RICO) and Small Cumulus Microphysics Study (SCMS). In particular, we consider droplet spectra averaged over segments of length, L, which may contain several clouds of varying size and liquid water density. We find evidence of spectral broadening that increases with L, and we use the spectra themselves, and not a correlation such as $\langle \langle r \rangle'_r \, w' \rangle$, to infer the L-dependence and size of $N_{\mathcal{D}}$.

7a. *Observational datasets*

i. RICO/SCMS Both the RICO and SCMS campaigns targeted fields of cumulus clouds with RICO focusing on shallow, maritime, trade wind cumulus while SCMS targeted shallow cumulus clouds in Florida. Both projects included the statistical sampling of cumulus cloud fields using a series of constant altitude

flight legs that attempt to gather a complete ensemble of cloud properties. Thus these data sets are well suited to the study of stochastic condensation. Our RICO analysis utilizes observations from 11 flights of the NCAR C-130 that targeted the statistical sampling of non-precipitating trade wind cumulus: RF-$\{$1,3,4,6,7,9,10,12,13,14,18$\}$ (JOSS 2005). For SCMS we use the same four NCAR C-130 flights analyzed and validated by Rodts et al. (2003) as a baseline: RF-$\{$12,13,16,17$\}$.

ii. Statistics The distribution of cloud sizes from RICO and SCMS is compared in Fig. 6(a) for cloud lengths between 100 and 7500 meters. Previous studies have shown that cumulus cloud sizes obey a power law distribution for sizes smaller than an outer length. This is verified in Fig. 6(a) which shows an increase in the decay of the size distribution beginning near ≈ 1000 m, consistent with previous results (Rodts et al. 2003).

We proceed to calculate cloud and droplet statistics averaged over segments of length $L_1 \leq L \leq L_2$ and over liquid water densities in the range, $\rho_1 \leq \langle \rho_l \rangle \leq \rho_2$. Statistics are calculated for six length bands: $L_1 \in 100, 200, 500, 1000, 2000, 5000$ and $L_2 \in 150, 300, 750, 1500, 3000, 7500$, respectively. For the RICO dataset four density bands (in $\mathrm{g/m^3}$) are selected: $\rho_1 \in \{0.01, 0.02, 0.05, 0.1\}$ and $\rho_2 \in \{0.02, 0.05, 0.1, 0.5\}$, respectively, while two density bands are chosen for SCMS: $\rho_1 \in \{0.02, 0.05\}$ and $\rho_2 \in \{0.05, 0.2\}$, respectively.

A plot of segment cloud fraction as a function of L is shown in Fig. 6(b). Segment cloud fraction decreases monotonically with increasing L as expected. It also increases monotonically with increasing $\langle \rho_l \rangle$ which reflects the fact that increasing cloud area, and not just increasing **in-cloud** liquid water density (see N_c above), is contributing to increase segment $\langle \rho_l \rangle$. As segment cloud fraction decreases with increasing L, we expect the number of clouds per segment to increase, and this is verified in Fig. 6(c). Unlike segment cloud fraction, no clear trend in cloud number with increasing $\langle \rho_l \rangle$ is evident. Figures 6(b) and (c) demonstrate good correspondence in the cumulus cloud statistics generated from the RICO and SCMS datasets. Overall, the SCMS segments contain somewhat fewer clouds and a significantly smaller cloud fraction than the RICO segments at a given $\langle \rho_l \rangle$.

The present model of stochastic condensation predicts increasing droplet spectral dispersion with increasing L. However, great care must be taken in the selection of an approximate statistic to measure this broadening in observational data. For our purposes, an appropriate measure of stochastic broadening must be insensitive to both the largest drops (which are affected by collision-coalescence) and the smallest (which are poorly measured by the FSSP-100). The width of the droplet radius spectrum from mode to Right-Quarter-Maximum (RQM) satisfies both of these criteria and is shown in Fig. 6(d) as a function of segment length L. Overall, Fig. 6(d) demonstrates increasing spectral dispersion (as measured by the width-at-RQM) with increasing L as expected from the theory of stochastic condensation. Increasing width-at-RQM with increasing $\langle \rho_l \rangle$ is also exhibited. Moreover, it is encouraging that the overall trend in width-at-RQM vs L is consistent across the RICO and SCMS datasets and density bands.

7b. *Spectral broadening and* $N_{\mathcal{D}}$

Atmospheric models are typically required to predict the evolution of the grid-cell averaged droplet spectrum, $f(r)$, or at least several of its moments, given a set of prognosed quantities at the grid-scale including $\langle \rho_l \rangle$. As shown in Figs. 6(b) and (c), a model grid-cell of (horizontal) size ≥ 100 meters containing cumulus will have a cloud fraction less than unity and may contain several clouds. Thus the grid-cell averaged spectrum will, in general, be distinct from the spectrum observed in, or averaged over, a single given cloud.

The six RICO spectra for density band 3, $0.05 \leq \langle \rho_l \rangle \leq 0.1$ in $\mathrm{g/m^3}$, are shown in Fig. 7(a) with unit normalization. The average single-measurement ($L =$ FSSP resolution) spectrum for the same $\langle \rho_l \rangle$ range is also reproduced (dotted line). Note that the local spectral maximum at 1.5 μm is in the small size regime where the FSSP-100 data quality is poor and is, subsequently, ignored. These spectra indicate that, for cumulus clouds, the shape of $f(r)$ is strongly L-dependent. This behavior is in contradistinction to the common modeling assumption that $f(r)$ obeys a log-normal or gamma distribution that is independent of L. In addition to the increase in width-at-RQM with increasing L documented in Fig. 6(d), Fig. 7(a) indicates a decrease in skewness with increasing L.

The observational spectra shown in Fig. 7(a) can be used to retrieve $\{N_z, N_{\mathcal{D}}\}$ using the present model of stochastic condensation in the QS limit, Eq. (22). We perform this retrieval by matching two statistics of the model to the data: (i) width-at-RQM and (ii) in-cloud mean radius, $\overline{r}$. The six retrieved spectra, corresponding to the six observational spectra for density band 3, are also shown in Fig. 7. Qualitatively, the two sets of spectra are similar with pronounced broadening in the "core" region between 3 and 15 μm that increases with increasing L. However, important differences are also evident. In particular, the observational spectra exhibit a sharp spectral peak between 3.5 and 6 μm that is

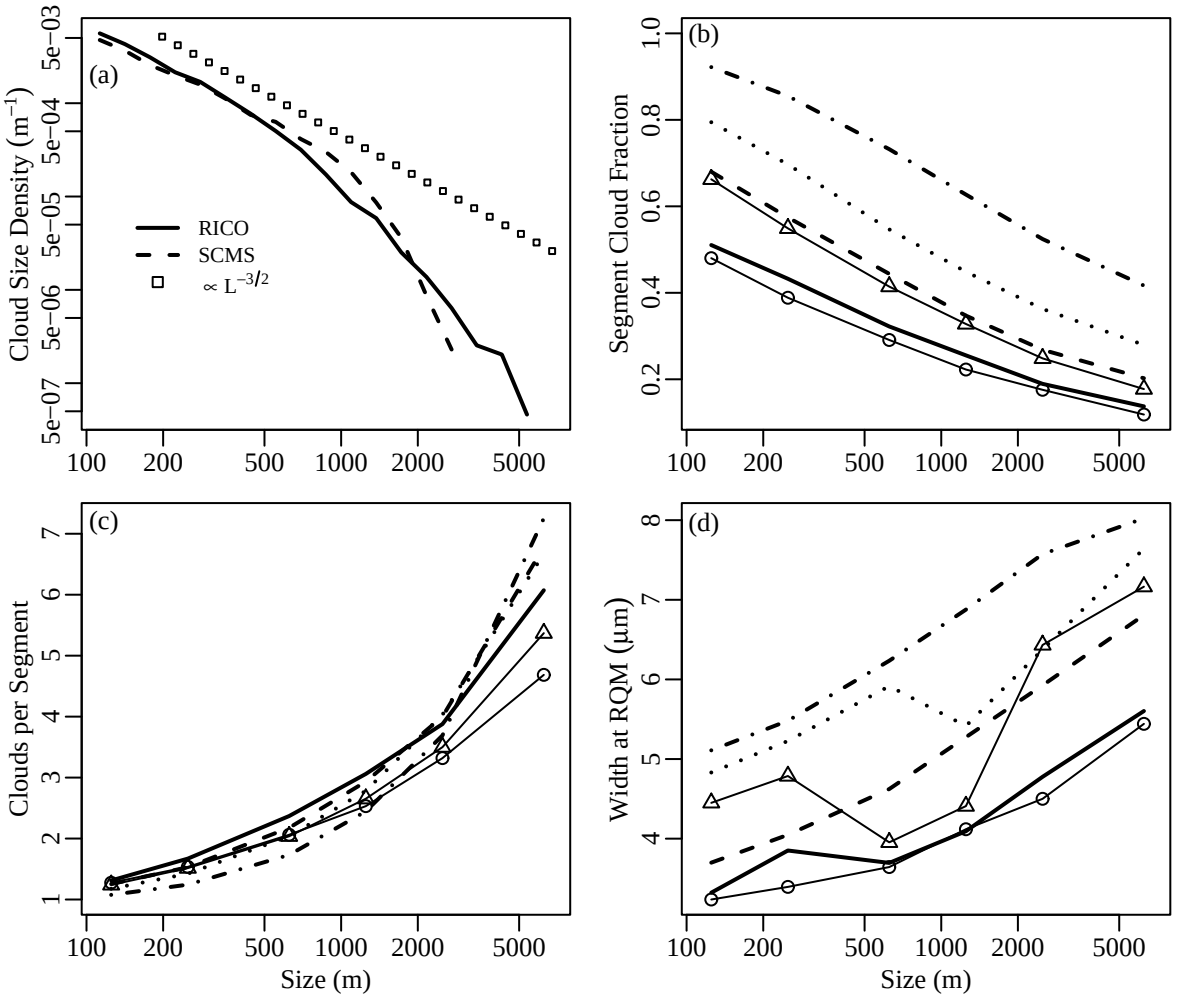

Figure 6: Cloud and droplet-spectrum statistics computed from the RICO and SCMS datasets described in the text using a cloud threshold of 7 cm^{-3} (Rodts et al. 2003). Fig 6(a) shows the distribution of cloud sizes between 100 and 7500 meters; a scale-break near 1000 m is evident (Rodts et al. 2003). For Figs. 6(b) through (d) the abscissa represents the length of an observational segment that may contain several clouds. Segment statistics are binned according to segment-averaged liquid-water density $\langle \rho_l \rangle$ (in g/m^3) for RICO (bold lines): 0.01–0.02 (—), 0.02–0.05 (- -), 0.05–0.01 ($\cdots$), 0.1–0.5 ($\cdot - \cdot$), and for SCMS (lines+symbols): 0.02–0.05 (◯), 0.05–0.2 (△). Cloud fraction, which decreases with increasing L, is shown in Fig. 6(b), while Fig. 6(c) shows cloud number which increases with increasing L. A comparison of spectral width at Right-Quarter-Maximum (RQM), computed from the segment-averaged droplet spectrum recorded by the FSSP-100, is given in Fig. 6(d). Spectral dispersion increases with increasing L, consistent with theoretical considerations of stochastic condensation from Sec. 5e.

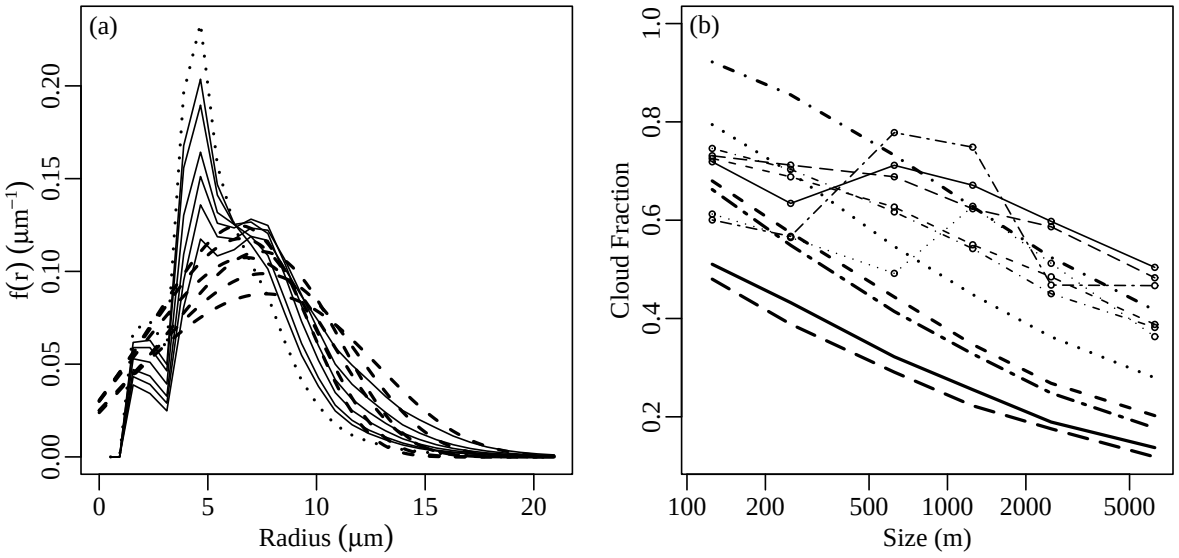

Figure 7: Comparison of observed droplet spectra [Fig. 7(a)] and cloud fraction [7(b)] vs model predictions. The observed spectra in 7(a) are computed for density band 3, $0.05 \leq \langle \rho_l \rangle \leq 0.1$ g/m^3: six spectra (—), corresponding to six L values (see text), and the single-point spectrum ($\cdots$) are shown, with the spectral peak decreasing monotonically with increasing L. Parameter values for the corresponding modeled spectra (- -), computed from Eq. (22), are retrieved by matching width-at-RQM and $\overline{r}$ to the observed values. Fig. 7(b) shows cloud fraction vs L for all observed (bold lines) and modeled (lines+symbols) density bands (in g/m^3) for RICO: 0.01–0.02 (—), 0.02–0.05 (- -), 0.05–0.01 ($\cdots$), 0.1–0.5 ($\cdot$–$\cdot$), and for SCMS: 0.02–0.05 (– –), 0.05–0.2 ($\cdot$—$\cdot$). The observed spectra and cloud fraction statistics show evidence of non-Gaussian S' statistics and inhomogeneous mixing, in contradistinction to the Levin-Sedunov-Mazin model of stochastic condensation.

not produced by the present model. In related fashion, the modeled spectra predict a significant fraction of droplets in the 0–3 μm regime that is not supported by the observations.

We attribute the cause of these differences to a key underlying assumption of the Levin-Sedunov-Mazin theory of stochastic condensation which can be phrased in two equivalent ways: (i) S', itself, is assumed normally distributed, as per Sec. 2, or (ii) the assumed Fokker-Planck renormalization $\tau \to 0$ gives a normal distribution of $\int_0^t \mathrm{d}\xi\, S'(\xi)$, independent of the S'-distribution. The equivalent result of either assumption is that a sizable portion of droplets experience a vanishingly small, but non-zero, negative supersaturation that permits them to exist in the 0–3 μm regime for extended periods before evaporating completely. This phenomenological picture is distinct from Baker et al. (1980)'s model of extreme inhomogeneous mixing in which a fraction of droplets evaporate completely during a mixing event while the remainder are unchanged. Thus Baker et al.'s model corresponds to a distribution of S' values that is strongly peaked near zero and near the negative supersaturation of unmixed environmental air. Support for this highly non-Gaussian distribution of S' values is found in a new PDF model of cloud mixing and evaporation (Jeffery and Reisner 2006).

Further support for non-Gaussian S' statistics and inhomogeneous mixing is found in Fig. 7(b) which shows a comparison of the observed cloud fractions, CF, (reproduced from Fig. 6(b)) and modeled cloud fractions, $\langle r^0 \rangle_r$. Strictly speaking, $\langle r^0 \rangle_r$ is not equivalent to observational CF; $f(r)$ does not provide spatial information and some volume fraction of the "labels" (e.g. CCN) of completely evaporated droplets may reside within cloudy air. Yet, overall, at large L the observational spectra exhibit, simultaneously, small cloud fractions (five out of six density bands with $0.1 < \mathrm{CF} < 0.3$) and well-defined spectral peaks, while the modeled spectra have larger cloud fractions ($0.35 < \langle r^0 \rangle_r \leq 0.5$) and significant broadening to smaller sizes. Thus Fig. 7(b) reiterates the importance of accounting for the inhomogeneous mixing processes—allowing for the complete evaporation of droplets **without** significant broadening to smaller sizes—in the formulation of stochastic mod-

els of grid-averaged spectra.

Lastly, the values of $N_{\mathcal{D}}$ retrieved from the observational RICO/SCMS spectra are shown in Fig. 8. Also shown in the figure is the theoretical estimate, $N_{\mathcal{D}} \sim L^{2/3}$, from Sec. 5e which assumes a constant, L-independent S'-variance. The pattern of retrieved $N_{\mathcal{D}}$ values shares similarities with the retrieved widths at RQM (Fig. 6(d)), although $N_{\mathcal{D}}$ does not exhibit a similar dependence on $\langle \rho_l \rangle$. For large scales, $L \geq 1000$ m, the retrieved $N_{\mathcal{D}}$ values are very consistent with the estimates of Fig. 4 for N_c around 50–150 cm^{-3} and T about 15–20 C°. This extremely encouraging result is the first observational confirmation of the stochastic condensation mechanism and the decades-old, work of Levin-Sedunov-Mazin. For smaller scales, $L < 1000$ m, the retrieved values of $N_{\mathcal{D}}$ appear to be overestimated. We attribute this overestimation to the lack of aerosol physics (sub-cloud distributions, activation, recycling) and collision-coalescence in the present approach which leads to a dispersion-less spectrum as $L \to 0$.

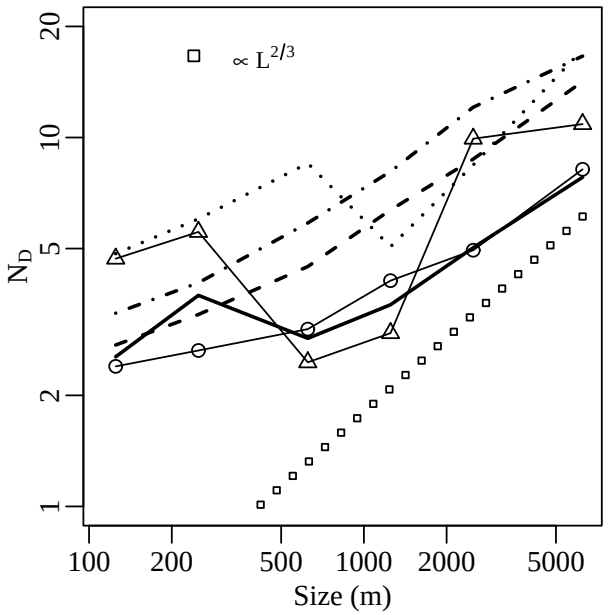

Figure 8: Retrieved values of $N_{\mathcal{D}}$ for all six segment lengths and all RICO (4) and SCMS (2) density bands. Line types for the six density bands as per Fig. 6(b)–(d); see Fig. 6 caption for further details. Also shown is the power-law relation $N_{\mathcal{D}} \sim L^{2/3}$ as a comparison. The retrieve $N_{\mathcal{D}}$ values agree well at large L with the estimates of Fig. 4 for $N_c \approx 50$–150 cm^{-3} and $T \approx 15$–20 C°.

8. SUMMARY

In this manuscript—which closely follows Jeffery et al. (2006)—we have taken "another look" at stochastic condensation in the hope of clarifying the earlier derivations and fully exploring the implications of this theory. In contrast to the derivations of Levin and Sedunov (1966a,b) and Manton (1979), we begin with a simple model of stochastic condensation—independent, Gaussian supersaturation fluctuations (S') renewed after a time τ—that is exactly solvable. This model is trivial to simulate on a computer and can be used to compare and contrast Lagrangian and Eulerian approaches for modeling droplet spectra (Andrejczuk et al. 2006). The Fokker-Planck approximation to this exact solution follows by replacing the discrete sampling of S' with its continuous surrogate. The Fokker-Planck diffusivity and operator are thus seen to be the natural smooth-in-time approximation to a discrete-in-time process.

We have also taken another look at the equation for the mean supersaturation, $\overline{S}_{\mathrm{FP}}$, in the presence of S' fluctuations modeled using the Levin-Sedunov-Mazin Fokker-Planck operator. While this problem is treated in an approximate fashion (and with little transparency) in Voloshchuk and Sedunov (1977), we derive the expression for $\langle S'|r \rangle_{\mathrm{FP}}$ without approximation and show how this expression "closes" the $\overline{S}_{\mathrm{FP}}$-equation self-consistently, thereby ensuring that total water mass is exactly conserved. Using the quasi-stationary (QS) evaluation of $\overline{S}_{\mathrm{FP}}$, we derive the exact correction term to $\overline{S}_{\mathrm{FP,QS}}$ (i.e. the S' contribution corresponding to the Levin-Sedunov-Mazin model). The correction term is negative definite, peaks in magnitude when $\langle r \rangle_r$ is near the accommodation length (≈ 2 μm), and decays as $\langle r^{-1} \rangle_r$ as the droplet spectrum grows to large sizes. This exact result has a direct correspondence to the analysis of Cooper (1989). Using our self-consistent equation for $\overline{S}_{\mathrm{FP}}$, we evaluate spectral broadening in an adiabatic parcel and find some broadening to larger sizes (consistent with earlier estimates, e.g. Manton (1979)), but a more significant decrease in $\langle r^2 \rangle_r$ at fixed liquid water content which may have implications for modeled cloud reflectivity.

While the proceeding discussion is largely a clarification and elucidation of previous work, most notably Voloshchuk and Sedunov (1977), we have also extended the theory of stochastic condensation by deriving the non-dimensional number, $N_{\mathcal{D}}$, that determines the relative impact of S'-fluctuations on droplet spectral evolution in an adiabatic volume and in the QS limit. For constant updraft velocity and Fokker-Planck diffusivity, $N_{\mathcal{D}}$ is also a constant, ranging from 10^{-2} to 10^2 for typical atmospheric conditions and model grid sizes when the assumed S'-standard deviation is 1%. We find sig-

nificant spectral broadening, and in particular decreasing $\langle r^2 \rangle_r$, for $N_{\mathcal{D}} > 1$, and discover that $\overline{S}_{\mathrm{FP,QS}}$ can be negative in a rising adiabatic parcel when $N_{\mathcal{D}} > 6.5$ for droplets of zero initial size.

Using in-situ droplet spectra from cumulus cloud fields observed during the RICO and SCMS field campaigns, we have verified a seminal prediction of the theory of stochastic condensation—increasing broadening with increasing spatial scale—by averaging the observed spectra over segments containing one or more clouds. In addition, scale-dependent values of $N_{\mathcal{D}}$ retrieved from the segment-averaged spectra using our adiabatic model show good consistency with the previously discussed theoretical estimates. We believe this encouraging result to be the first observational confirmation of the stochastic condensation mechanism and the decades-old, pioneering work of Levin-Sedunov-Mazin. Moreover, these results suggest that the parameterization of unresolved S'-fluctuations using Fokker-Planck theory or other means will become increasingly important as explicit (bin) microphysics schemes are applied at larger scales (Lynn et al. 2005), where an increasing fraction of individual clouds are, themselves, unresolved.

However, important differences between the observed and modeled droplet spectra are also observed. In particular, the observed spectra suggest non-Gaussian S' fluctuations and the inhomogeneous mixing process of Baker et al. (1980). Further work is needed to assess the impact of non-Gaussian S'-fluctuations and large renewal times on droplet spectral broadening and to derive differential operators that can model their ensemble effect in the equations of cloud physics.

Acknowledgement This work was funded by a Los Alamos National Laboratory Directed Research and Development Project entitled “Resolving the Aerosol-Climate-Water Puzzle (20050014DR)”. The lead author is indebted to the “Crisis Points” program (1996-2000) of the Peter Wall Institute for Advanced Studies which provided the foundation for this work.

A. THERMODYNAMICS CONSTANTS

The constant α defined in Eq. (3) is (Pruppacher and Klett 1997, Eq. (13-28))

$$\alpha = (\rho_s/\rho_w) D_v G$$

where

$$G = \left\{ 1 + \frac{\rho_s}{\rho_d} \frac{L_v}{c_p T} \left(\frac{L_v}{R_v T} - 1 \right) \right\}^{-1},$$

ρ_s is saturation vapor density, ρ_d is air density, ρ_w is water density, D_v is molecular diffusivity of vapor, L_v is latent heat of vaporization, c_p is heat capacity, R_v is water vapor gas constant, T is temperature, and we have assumed equality of the conductivities of vapor and temperature.

The constant c_1 of Eq. (17) is (Pruppacher and Klett 1997, Eq. (13-29))

$$c_1 = \frac{L_v}{R_v T^2} \frac{g}{c_p} - \frac{g}{R_d T}$$

where g is gravitational acceleration and R_d is the gas constant of air. To good approximation the constant c_2 is

$$c_2 = (4/3)\pi D_v N_c / \alpha$$

where N_c is droplet concentration.

REFERENCES

Andrejczuk, M., J. M. Reisner, and C. A. Jeffery, 2006: Comparison of analytical solutions for the growth of cloud droplets against Eulerian and Lagrangian numerical formulations. *J. Atmos. Sci.*, submitted.

Austin, P. H., M. B. Baker, A. M. Blyth, and J. B. Jensen, 1985: Small-scale variability in warm continental cumulus clouds. *J. Atmos. Sci.*, **42**, 1123–1138.

Baker, M. B., R. G. Corbin, and J. Latham, 1980: The influence of entrainment on the evolution of cloud droplet spectra: I. A model of inhomogeneous mixing. *Quart. J. Roy. Meteor. Soc.*, **106**, 581–599.

Bartlett, J. T. and P. R. Jonas, 1972: On the dispersion of the sizes of droplets growing by condensation in turbulent clouds. *Quart. J. R. Met. Soc.*, **98**, 150–164.

Belyaev, V. I., 1961: The size distribution of drops in a cloud in the condensation stage of development. *Bull. (Izv.) Acad. Sci. USSR, Geophys. Ser.*, **8**.

Cooper, W. A., 1989: Effects of variable droplet growth histories on droplet size distributions. Part I: Theory. *J. Atmos. Sci.*, **46**, 1301–1311.

Han, Q., W. B. Rossow, and A. A. Lacis, 1994: Near-global survey of effective droplet radii in liquid water clouds using ISCCP data. *J. Climate*, **7**, 465–497.

Heymsfield, A. J. and G. M. McFarquhar, 2001: Microphysics of INDOEX clean and polluted trade cumulus clouds. *J. Geophys. Res.*, **106**, 28653–28673.

Jeffery, C. A. and J. M. Reisner, 2006: A study of cloud mixing and evolution using PDF methods. 1. Cloud front propagation and evaporation. *J. Atmos. Sci.*, in press.

Jeffery, C. A., J. M. Reisner, and M. Andrejczuk, 2006: Another look at stochastic condensation in clouds: Exact solutions, Fokker-Planck approximations and adiabatic evolution. *J. Atmos. Sci.*, in review.

JOSS, 2005: RICO mission table, `http://www.joss.ucar.edu/rico/catalog/missions`.

Khvorostyanov, V. I., 1988: A kinetic equation for stochastic condensation with analytical solutions of the gamma-distribution type. *Atmos. Ocean. Phys.*, **24**, 134–141.

Khvorostyanov, V. I. and J. A. Curry, 1999a: Toward the theory of stochastic condensation in clouds. Part I: A general kinetic equation. *J. Atmos. Sci.*, **56**, 3985–3996.

— 1999b: Toward the theory of stochastic condensation in clouds. Part II: Analytical solutions of the gamma-distribution type. *J. Atmos. Sci.*, **56**, 3997–4013.

Levin, L. M. and Y. S. Sedunov, 1966a: A kinetic equation describing microphysical processes in clouds. *Doklady Akad. Nauk SSSR*, **170**, 4–6.

— 1966b: Stochastic condensation of drops and kinetics of cloud spectrum formation. *J. Rech. Atmos.*, **2**, 425–432.

— 1967: Kinetics of the formation of a cloud spectrum. *Atmos. Ocean. Phys.*, **3**, 242–248.

Lynn, B. H., A. P. Khain, J. Dudhia, D. Rosenfeld, A. Pokrovsky, and A. Seifert, 2005: Spectral (bin) microphysics coupled with a mesoscale model (MM5). Part I. Model description and first results. *Mon. Wea. Rev.*, **133**, 44–58.

Manton, M. J., 1979: On the broadening of a droplet distribution by turbulence near cloud base. *Quart. J. R. Met. Soc.*, **105**, 899–914.

Mazin, I. P., 1965: Theory of formation of a particle-size spectrum in clouds and precipitation. *Trans. (Trudy) Central Aerological Observatory*, **64**.

Politovich, M. K., 1993: A study of the broadening of droplet size distributions in cumuli. *J. Atmos. Sci.*, **50**, 2230–2244.

Pruppacher, H. R. and J. D. Klett, 1997: *Microphysics of Clouds and Precipitation*. Kluwer Academic, Boston, MA, USA, 2nd edition.

Risken, H., 1989: *The Fokker-Planck Equation*. Springer-Verlag, Berlin, Heidelberg, New York, 2nd edition.

Rodts, S. M. A., P. G. Duynkerke, and H. J. J. Jonker, 2003: Size distributions and dynamical properties of shallow cumulus clouds from aircraft observations and satellite data. *J. Atmos. Sci.*, **60**, 1895–1912.

Sedunov, Y. S., 1965: Fine cloud structure and its role in the formation of the cloud particle spectrum. *Atmos. Ocean. Phys.*, **1**, 416–421.

Sutton, O. G., 1953: *Micrometeorology*. McGraw-Hill.

Vaillancourt, P. A., M. K. Yau, P. Bartello, and W. W. Grabowski, 2002: Microscopic approach to cloud droplet growth by condensation. Part II. turbulence, clustering, and condensational growth. *J. Atmos. Sci.*, **59**, 3421–3435.

Vaillancourt, P. A., M. K. Yau, and W. W. Grabowski, 2001: Microscopic approach to cloud droplet growth by condensation. Part I: Model description and results without turbulence. *J. Atmos. Sci.*, **58**, 1945–1964.

Voloshchuk, V. M. and Y. S. Sedunov, 1977: The kinetic equation of drop-spectrum evolution in the turbulent medium for the condensed stage in cloud development. *Sov. Meteor. Hydrol.*, **3**, 1–10.